Available online at www.sciencedirect.com
SCIENCE DIRECT®
Catalysis Today 97 (2004) 13–23
CATALYSIS TODAY
www.elsevier.com/locate/cattod

Characterization of extraframework aluminum in H-mordenite dealuminated with ammonium hexafluorosilicate

Hsien-Ming Kao [a,*], Yun-Chu Chen [a], Chun-Chiang Ting [a], Po Tuan Chen [b], Jyh-Chiang Jiang [b]

[a] *Department of Chemistry, National Central University, Chung-Li 32054, Taiwan*
[b] *Department of Chemical Engineering, National Taiwan University of Science and Technology, Taiwan*

Received 16 November 2003; accepted 29 January 2004
Available online 10 August 2004

Abstract

The status and nature of extraframework Al (EFAl) species in H-mordenite dealuminated by ammonium hexafluorosilicate (i.e., $(NH_4)_2SiF_6$, AHFS) was investigated. Considerable difference arising from the experimental conditions of AHFS dealumination, that is, in the presence and absence of ammonium acetate (NH_4OAc), was observed. Both treatments were not very effective in removing framework aluminum. ^{27}Al and ^{19}F solid-state NMR was used to detect different extraframework aluminum fluoro-complexes resulting from the AHFS dealumination. In the presence of NH_4OAc, the essential part of the dealumination process carried on with AHFS was that most of the extracted Al^{3+} reacted with F^- to form $(NH_4)_3AlF_6$. In the absence of NH_4OAc, on the other hand, at least two different forms of aluminum fluoro-complexes other than $(NH_4)_3AlF_6$ were formed after dealumination. These aluminum fluoro-complexes showed multiple lines located in the range of −144 to −156 ppm in the ^{19}F NMR spectrum. An ab initio method that used both Hartree-Fock and hybrid Hartree-Fock density functional methods at the 6-31+G* basis set level was used to calculate the ^{19}F NMR shifts for discriminating possible aluminum fluoro-complexes. Our results indicated that a combination of NMR and ab initio calculations provided a basis for using them to study EFAl species of unknown compositions and structures.

Keywords: Ab initio calculation; Dealumination; Extraframework aluminum species; Mordenite; Solid-state NMR

1. Introduction

The nature and strength distribution of acid sites in zeolites can significantly vary with the aluminum content that can be controlled by the methods of dealumination, a process that removes framework aluminum atoms without severely destroying the micropore structure of zeolites. Dealumination of zeolites allows adjustments in the Si/Al ratio of zeolites, hence their acidity and catalytic properties. For example, the dealumination of zeolite Y not only improves its hydrothermal stability but also influences its catalytic cracking properties [1]. Dealumination by steaming [2], leaching with acids such as HCl [3], oxalic acid [4], or critic acid [5], and by reaction with chemical agents such as silicon tetrachloride [6] or ammonium hexafluorosilicate, $(NH_4)_2SiF_6$ (AHFS) [7,8] are some common post-synthesis techniques used to control the acidity of zeolites. Depending on the methods used for dealumination, acidic properties of zeolites may be changed dramatically, often accompanied by a substantial amount of extraframework aluminum (EFAl) species formed inside the zeolite structure. Different zeolite structure types, such as Beta, mordenite (MOR), Y, and ZSM-5, have been reported to exhibit a very different behavior towards the various dealumination methods [9]. The properties and performance of zeolites usually depend on the state of the aluminum species in the zeolites, and therefore, the investigation of the state of aluminum after dealumination is significant and interesting.

Mordenite is a large pore zeolite and possesses a two-dimensional network of channels consisting of straight 12-membered ring pores (6.4 Å × 7.2 Å) connected by twisted 8-membered pores of 2.6 Å × 5.7 Å side pockets [10]. In spite of extensive dealumination of zeolites by

* Corresponding author. Tel.: +886-3-4275054; fax: +886-3-4227664.
E-mail address: hmkao@cc.ncu.edu.tw (H.-M. Kao).

0920-5861/$ – see front matter © 2004 Elsevier B.V. All rights reserved.
doi:10.1016/j.cattod.2004.01.007

various methods, only a limited number of studies have focused on the dealumination of zeolites with AHFS, since it is relatively mild dealumination agent. The influence of the treatment of mordenite by AHFS on physicochemical and catalytic properties has been reported [11]. The AHFS dealumination method has the advantage, in comparison with the other dealumination methods, that silicon atoms can directly replace the extracted aluminum atoms while still maintaining much of the crystallinity of the sample. According to the standard AHFS dealumination method reported by Skeels and Breck [7,8], the zeolite samples were dealuminated in the presence of ammonium acetate (NH_4OAc), followed by washing with hot water. Consequently, the resulting samples were almost free of extraframework Al species. This could be beneficial in avoiding the blockage of the acid sites from EFAl species that can be located either on the outer surface or inside the channels of zeolites. The removal of EFAl species by washing with hot water, however, is not appropriate for the fundamental study of EFAl species formed during the dealumination. Little attempt has been made to characterize the status and exact nature of EFAl species induced by AHFS treatment.

The nature of EFAl species has been the subject of much interest and two forms have been proposed in the literature [12]: cationic particles adsorbed in anionic zeolites, e.g., Al^{3+}, AlO^{+}, $Al(OH)^{2+}$, and $Al(OH)_2{}^{+}$, and neutral or polymeric aluminum species, e.g., $AlO(OH)$, $Al(OH)_3$, and Al_2O_3. Although computational methods have been widely used in describing the structure, acidity, and catalytic performance of zeolites, there are only few studies simulating EFAl structures of dealuminated zeolites [13–18]. With the rapid increase of computer power, the ab initio molecular orbital calculation method is becoming increasingly reliable in predicting geometry and NMR properties. For example, a density functional theory (DFT) was recently employed to study the structure of extraframework Al species such as Al^{3+}, AlO^{+}, $Al(OH)_2{}^{+}$, $AlO(OH)$, and $Al(OH)_3$ in zeolites [18]. More recently, Liu et al. reported theoretical calculations of ^{19}F NMR shifts for possible Al–F species in fluorine-bearing aluminosilicate glasses [19].

This study aimed at a better understanding of the unique effects that AHFS treatment, in the presence and the absence of NH_4OAc, induced on the status and nature of EFAl species in dealuminated H-MOR zeolites. The dealuminated samples were characterized with a variety of techniques such as powder X-ray diffraction (XRD), multinuclear solid-state NMR (^{27}Al, ^{19}F, and ^{29}Si), and cumene cracking activity measurements. In particular, NMR has been recognized as a powerful tool for the identification of the variation of short-range ordering of the zeolite structure and for the characterization of EFAl species. The lack of theoretical studies for describing the structure and ^{19}F NMR shifts of EFAl species in dealuminated zeolites prompted us to carry out ab initio calculations for ^{19}F NMR shifts of EFAl species. To help the assignment of ^{19}F NMR peaks, we reported here preliminary results of ^{19}F NMR shifts concerning some possible structures of six-coordinated extraframework Al species containing terminal F atoms.

2. Experimental

2.1. Sample preparation

The parent zeolite H-MOR was prepared from NH_4-MOR, with a Si/Al ratio of 10 and obtained from Zeolyst, by slowly ramping the temperature of sample to 400 °C over a period of 6 h in air; the sample was kept at this temperature for another 12 h. The standard AHFS method of Skeels and Breck [7,8] was slightly modified to dealuminate H-MOR. Two series of dealuminated samples were prepared. First, 1 g of H-MOR was preheated at 80 °C in a 50 ml of 3.0 M aqueous solution of NH_4OAc. The initial pH of the zeolite solution was approximately 7, and was then lowered to about 6.5 by the dropwise addition of 10 ml aqueous AHFS solution with various concentrations over a period of 1 h. The solution was then kept at 80 °C with constant stirring for another 3 h. The resulting solution was cooled to room temperature, filtered, and then dried, *without prior washing*, in an oven at 60 °C overnight. In contrast to the standard procedure of AHFS treatment, dealuminated samples were not washed by hot water in order to fully characterize all the EFAl and fluorinated species formed after dealumination. However, some water-soluble aluminum fluorides might be lost during filtration. As a result, the bulk Si/Al molar ratio of dealuminated samples, determined by ICP-AES, was slightly increased (in the range of 11.0–12.5) as compared to that of the parent H-MOR sample. The amount of AHFS was chosen to obtain a molar ratio of AHFS to the total Al content of the parent zeolite varying from 0.5 to 5.0. These dealuminated samples were designated as H-MOR/AHFS-*x*-NH_4OAc, where *x* denotes the molar ratio of AHFS to the total Al content of the parent zeolite. It was reported that experimental parameters such as pH were critical on the extent and nature of the dealumination [7,8]. For comparison, another series of dealuminated samples were prepared by the same procedure without adding NH_4OAc. The final pH of the suspension prepared in this way was approximately 3.5. These dealuminated samples were labeled as H-MOR/AHFS-*x*-None.

2.2. Characterization

Powder X-ray diffraction patterns from $2\theta = 5$–60° were collected on a Shimadzu XRD-6000 diffractometer using Cu Kα radiation ($\lambda = 1.5406$ Å) to determine crystallinity as well as lattice parameters. Crystallinities were estimated by comparing the sum of the intensities of X-ray diffraction peaks of AHFS-treated H-MOR samples with that of the parent H-MOR sample. ^{19}F and ^{27}Al magic angle spinning

(MAS) NMR spectra were recorded on a Bruker DSX-300 spectrometer equipped with a 4 mm MAS probe with resonance frequencies of 282.2 and 78.2 MHz, respectively. All ^{27}Al MAS NMR spectra were obtained with small flip angles of approximately 15° and with a recycle delay of 3 s under identical experimental conditions in order to make a quantitative comparison of the number of ^{27}Al spins [20]. To investigate the effect of hydration on the status and nature of aluminum in dealuminated zeolites, the dealuminated samples were exposed to an ambient atmosphere to reach various hydration levels. The as-synthesized samples, obtained from thermal treatment of samples in oven at 60 °C, were hydrated for one day to become "partially hydrated" samples. These partially hydrated samples were further hydrated for a week to become "fully hydrated" samples. ^{19}F MAS NMR spectra were recorded on the partially hydrated samples to avoid possible huge ^{19}F–^{19}F homonuclear dipolar couplings, and acquired with a $\pi/2$ pulse of 4.5 μs, a recycle delay of 15 s, and at a spinning speed of 12 kHz. A Hahn echo sequence was applied for refocusing the magnetization lost in the dead time and the signal distorted by the probe. Several thousand scans were accumulated. The ^{19}F and ^{27}Al chemical shifts were externally referenced to $CFCl_3$ and $Al(H_2O)_{6(aq)}^{3+}$ at 0.0 ppm, respectively. Simulations of ^{27}Al NMR lineshapes were performed with the WINFIT program of the Bruker WINNMR software package to extract both the qradrupole coupling constant (QCC) and the asymmetry parameter (η). Additional interactions such as ^{27}Al–^{19}F dipolar coupling were not taken into account. A $\pi/6$ pulse length of 2.5 μs and a repetition time of 10 s were used in the ^{29}Si MAS NMR experiments. ^{29}Si chemical shifts were externally referenced to tetramethylsilane (0.0 ppm). Cumene cracking reaction was performed in a continuous-flow fixed-bed reactor (quartz) system with N_2 (40 mL min^{-1}) as a carrier gas. The catalyst load for the tests was 100 mg and was pretreated in a flow of nitrogen at 500 °C for 3 h. Cumene was introduced by passing a flow of nitrogen through a bubble containing liquid cumene at room temperature. The products were analyzed by an on-line gas-chromatographic system equipped with a flame ionization detector.

2.3. Calculation methods

All calculations were performed using Gaussian'98 program [21]. We employed the density functional theory calculations with the hybrid B3LYP method [22] and the standard 6-31+G* basis set, to provide fully optimized geometries without symmetry constraint of the six-coordinated extraframework Al species containing terminal F atoms. The stable minima (number of imaginary frequencies NIMAG = 0) were confirmed through the calculations of harmonic vibrational frequencies. NMR shielding tensors were calculated using the GIAO (gauge-including atomic orbital) method [23,24], which was used as the default NMR method in Gaussian'98. Using the GIAO formalism, the isotropic shielding (σ_{iso}) was obtained by averaging the three principal tensor components σ_{11}, σ_{22}, and σ_{33}. In order to reference the calculated chemical shifts with respect to a standard, GIAO calculations were also carried out on $CFCl_3$. Isotropic chemical shifts (δ_{iso}) were calculated using the relationship $\delta_{iso} = \sigma_{iso}^{ref} - \sigma_{iso}^{sample}$, where σ_{iso}^{ref} is the chemical shielding value of the reference substance, $CFCl_3$, calculated at the same level.

3. Results and discussion

3.1. XRD studies

Fig. 1 shows the XRD patterns of dealuminated samples, along with the parent H-MOR sample. The XRD powder patterns showed that all dealuminated samples still retained about 75% of their crystallinities after dealumina-

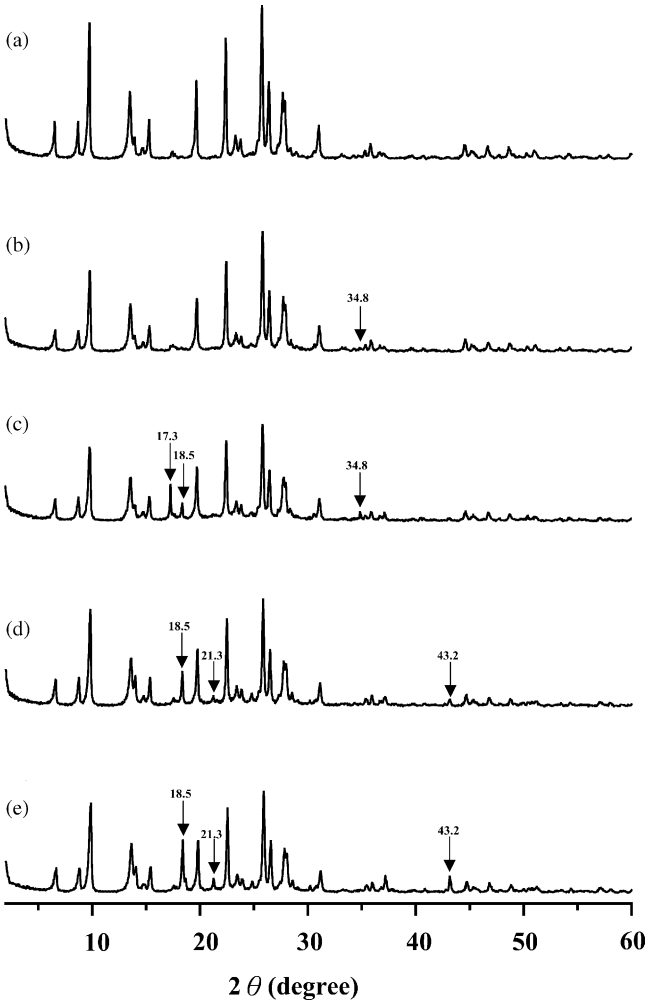

Fig. 1. XRD patterns of (a) H-MOR, (b) H-MOR/AHFS-1.5-NH_4OAc, (c) H-MOR/AHFS-5.0-NH_4OAc, (d) H-MOR/AHFS-1.5-None, and (e) H-MOR/AHFS-5.0-None.

tion. The treatment of the H-MOR with AHFS has practically no effect on the unit cell parameters. This showed that zeolite mordenite was stable against AHFS dealumination. At high AHFS loading, however, the XRD powder patterns did provide additional information. In the case of H-MOR/AHFS-5.0-NH_4OAc, two new peaks at $2\theta = 17.3^\circ$ and 18.5° were observed (Fig. 1c), while several new peaks at $2\theta = 18.5^\circ$, 21.3°, 34.8°, and 43.2° were observed in the case of H-MOR/AHFS-5.0-None sample (arrows in Fig. 1e). The peak at $2\theta = 17.3^\circ$ can be ascribed to the formation of $(NH_4)_3AlF_6$ phase at high AHFS loading in the presence of NH_4OAc. Other peaks are possibly due to the formation of minute amounts of AlF_xO_y phase.

3.2. ^{27}Al MAS NMR of H-MOR/AHFS-x-NH_4OAc

^{27}Al MAS NMR has been widely used to determine the coordination and the local structure of specific aluminum species in zeolites since both tetrahedral and octahedral ^{27}Al sites can be readily resolved based on their distinctly different chemical shifts. When the aluminum atoms are tetrahedrally coordinated to the framework of zeolites, then a resonance in the range of 50–60 ppm is visible in the ^{27}Al NMR spectrum. Dealumination would result in some EFAl species. EFAl species are usually octahedrally coordinated, and the responding signal has a chemical shift at around 0 ppm. Thus the ^{27}Al MAS NMR spectra can yield valuable information on the dealumination of zeolitic framework. The disadvantage of the ^{27}Al MAS NMR method is that some of the Al atoms may be invisible, especially in a fully dehydrated zeolite sample, because of a large quadrupolar interaction with the electric field gradient at the ^{27}Al nucleus spin that is sited in a distorted environment. The studied zeolite samples were, therefore, exposed to an ambient atmosphere to reach different hydration levels before ^{27}Al MAS NMR measurements.

Fig. 2 displays the ^{27}Al MAS NMR spectra of H-MOR, and partially hydrated samples dealuminated by AHFS in the presence of NH_4OAc. The ^{27}Al MAS NMR spectrum of H-MOR revealed two resonances at 55 and 0 ppm due to aluminum atoms in the tetrahedral and octahedral environments, respectively (Fig. 2a). This dealumination occurred during the calcinations, because the aluminum atoms in the framework were not stabilized very well by the protons. With addition of AHFS ($x = 1.5$, Fig. 2b), a slight decrease in the intensity of the resonance at 55 ppm accompanied by the appearance of a new broad peak at 13 ppm was observed, indicating that some framework aluminum was expelled from the framework. In addition, the peak at 0 ppm became sharper. Following the standard AHFS treatment, i.e., the dealuminated samples was further washed with hot water, the peak due to octahedrally coordinated Al (13 and 0 ppm) disappeared and only tetrahedral coordinated Al existed. This implied that these octahedral Al species were EFAl species. No new spectral feature was observed with higher AHFS contents ($x = 5.0$), except an increase in the intensity of the peak at 0 ppm (Fig. 2c). The narrow linewidth of the resonance at 0 ppm indicated that the aluminum atom in EFAl species possessed a very symmetrical environment. In contrast, the larger linewidth for the resonance at 13 ppm implied a stronger quadrupolar interaction at this aluminum site, and thus a more distorted environment. It was also possible that the broad peak at 13 ppm consisted of a distribution of different EFAl species with similar chemical shifts. A close inspection of the ^{27}Al spectrum shown in Fig. 2b revealed the existence of a small broad peak at around −5 ppm, which was underneath the peak at 0 ppm. This broad peak resulted from further hydration of the species resonating at 13 ppm, which will be shown later. Unfortunately, this peak overlapped with the sideband resulting from the peak at 55 ppm in the spectrum of Fig. 2c under the experimental conditions. The spectrum obtained at a higher spinning speed (e.g., 12 kHz) confirmed the presence of the peak at −5 ppm in H-MOR/AHFS-5.0-NH_4OAc as well. As evidenced in the ^{27}Al MAS NMR spectra shown in Fig. 2, at least two different types of EFAl species resonating at 13 and 0 ppm were present in H-MOR/AHFS-x-NH_4OAc samples.

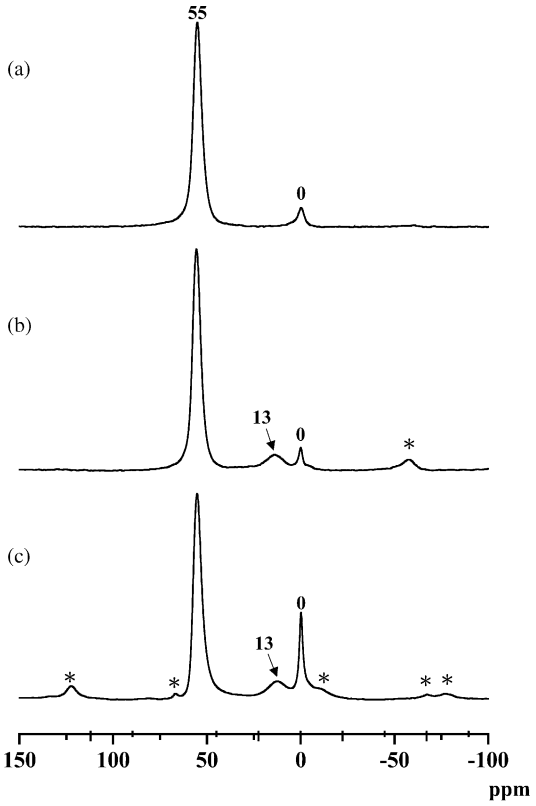

Fig. 2. ^{27}Al MAS NMR spectra of partially hydrated (a) H-MOR, (b) H-MOR/AHFS-1.5-NH_4OAc, and (c) H-MOR/AHFS-5.0-NH_4OAc samples, acquired at a spinning speed of 7 (c) or 12 (a, b) kHz. Asterisks denote spinning sidebands. The spectra are not normalized.

3.3. ^{27}Al MAS NMR of H-MOR/AHFS-x-None

The ^{27}Al MAS NMR spectra of AHFS treated H-MOR in the absence of NH_4OAc as a function of AHFS content are shown in Fig. 3. At a low level of AHFS ($x = 0.5$), besides framework aluminum at 55 ppm, a broad peak centered at around 13 ppm was observed (Fig. 3a). In the case of H-MOR/AHFS-2.5-None sample (Fig. 3b), however, an additional sharp peak at 0 ppm with a shoulder at −5 ppm appeared. A close examination of the spectrum indicated the presence of a much broader pattern spread from −20 to −90 ppm, which was enlarged as indicated in the inset of Fig. 3b. The broad pattern, induced by the second-order quadrupolar interaction, must be associated with an aluminum site with large quadrupolar interaction. Note that the middle part of the broad pattern overlaps with the first-order sideband from the peak at 55 ppm. By assuming that there is no distribution for this site, a simulation of its lineshape readily yields NMR parameters: isotropic chemical shift $\delta_{iso} = -5 \pm 2$ ppm, C_Q (quadrupole coupling constant) $= 9.5 \pm 0.3$ MHz, and η_Q (quadrupole asymmetry parameter) $= 0.1 \pm 0.1$. The simulated spectrum is also shown as dashed line, together with the spinning sideband, in the inset of Fig. 3b. The large C_Q for this EFAl species is indicative of a more distorted aluminum environment. The resonance at 13 ppm was no longer observed and the pattern spread from –20 to –90 ppm was still observable in the ^{27}Al spectrum at a higher AHFS loading ($x = 5.0$, Fig. 3c). The low intensity of this peak excludes any possibility for ^{27}Al MQMAS NMR experiments [25]. As evidenced in Fig. 3, there are three major types of EFAl, namely the resonances at 13, 0 ppm, and the pattern spread from −20 to −90 ppm, present in the AHFS treated H-MOR in which no NH_4OAc was added. The ^{27}Al NMR results, as shown in Figs. 2 and 3, demonstrated that the exact experimental procedures of AHFS dealumination, that is, in the presence and absence of NH_4OAc in this case, strongly affected the amount, state, and nature of EFAl species.

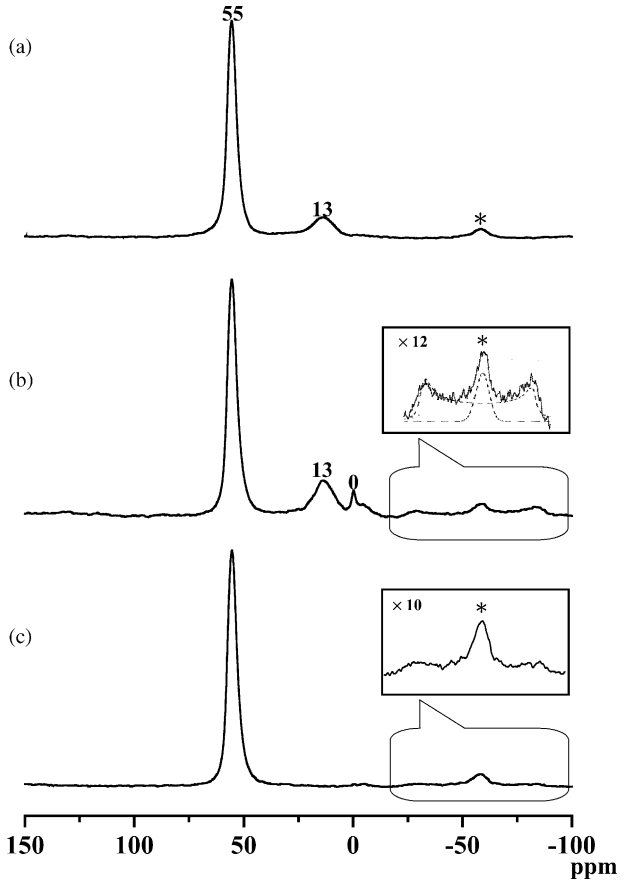

Fig. 3. ^{27}Al MAS NMR spectra of partially hydrated H-MOR/AHFS-*x*-None, where *x* is equal to (a) 1.5, (b) 2.5, and (c) 5.0, acquired at a spinning speed of 12 kHz. Asterisks denote spinning sidebands. The spectra are not normalized.

3.4. Effect of hydration level on the ^{27}Al spectrum

To investigate the hydration level on the state of EFAl species, dealuminated samples were exposed to atmospheric moisture and their ^{27}Al spectra were compared. Few octahedral aluminum species at 0 ppm were observed in the ^{27}Al NMR spectrum of as-synthesized H-MOR/AHFS-1.5-NH_4OAc sample (Fig. 4a). However,

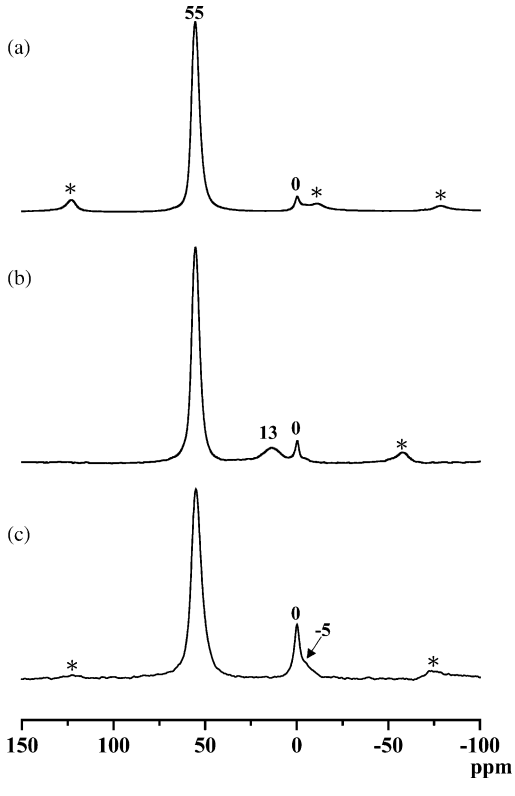

Fig. 4. ^{27}Al MAS NMR spectra of H-MOR/AHFS-1.5-NH_4OAc at different hydration levels: (a) as-synthesized, (b) partially hydrated, and (c) fully hydrated. Spectra (a) and (c) were acquired at a spinning speed of 12 kHz, and (b) at a spinning speed of 7 kHz. Asterisks denote spinning sidebands.

when the sample was analyzed after exposure to atmospheric moisture to become partially hydrated, the peak at 13 ppm appeared (Fig. 4b). This suggested that the initial state of the aluminum species for the peak at 13 ppm was "invisible", and becomes visible after coordination with water molecules. Interestingly, the peak at 13 ppm present in the partially hydrated sample disappeared after a further hydration period of 1 week (fully hydrated), and simultaneously the sharp peak at 0 ppm was superposed by a broad signal at around −5 ppm (Fig. 4c). The presence of the broad component at around −5 ppm was evident from its corresponding broad spinning sidebands. For dealuminated samples in the absence of NH_4OAc, the same behavior for the peak at 13 ppm was observed. In contrast, the broad pattern spread from −20 to −90 ppm appeared to be unaltered upon hydration. Clearly, the nature and state of EFAl species for the peak at 13 ppm changed as a function of hydration level of the sample.

3.5. Degree of dealumination

As demonstrated above, quantification of the total Al content in these dealuminated samples was complicated by the moisture content and compositional changes during the treatments. Some errors might occur because of the loss of some water-soluble aluminum fluorides during filtration. Furthermore, the quadrupolar effects of the aluminum nuclei should also be taken into account. The dealumination with a total amount of AHFS corresponding to 100% of total aluminum content of H-MOR resulted in only approximately 13% dealumination for both treatments. In a previous work on the dealumination of ZSM-5 and Y zeolites in the presence of NH_4OAc, AHFS removed 24 and 50% framework aluminum atoms if a total amount of AHFS corresponding to 100% of its framework aluminum atoms was used [26]. Therefore, zeolite mordenite is more resistant to AHFS dealumination than zeolites Y and ZSM-5. Extensive treatment with an excess of AHFS ($x = 5.0$) resulted in a further dealumination up to ∼25% in the presence of NH_4OAc while no further dealumination was observed in the absence of NH_4OAc.

3.6. ^{19}F MAS NMR of H-MOR/AHFS-x-NH_4OAc

Fig. 5 shows the ^{19}F MAS NMR spectra of H-MOR/AHFS-*x*-NH_4OAc as a function of AHFS content. At low level of AHFS ($x = 1.5$), three major peaks at −130, −143, and −156 ppm were observed. The peak at –130 ppm can be assigned to unreacted SiF_6^{2-} and the small peak at −125 ppm is presumably due to the presence of the F^- counterion of NH_4^+ or H^+ occurring in channels [27]. The resonance at −156 ppm appeared to be associated with some shoulders in the range of −150 to −152 ppm and a small peak at −161 ppm. The peak at −143 ppm dominated the spectrum whereas a broad, less intense peak centered at −156 ppm with low-field shoulders

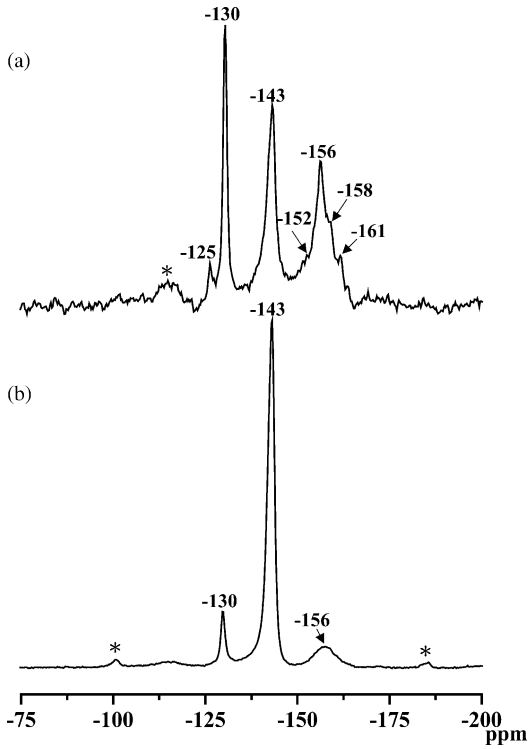

Fig. 5. ^{19}F MAS NMR spectra of H-MOR/AHFS-*x*-NH_4OAc, where *x* is equal to (a) 1.5 and (b) 5.0. Spectra were acquired at a spinning speed of 12 kHz. Asterisks denote spinning sidebands.

was observed as the amount of AHFS was further increased ($x = 5.0$, Fig. 5b). Since the major EFAl species observable in the corresponding ^{27}Al spectrum was at 0 ppm, the peak at −143 ppm in the ^{19}F NMR spectrum must be associated with this EFAl species. The peak at −143 ppm is assigned to $(NH_4)_3AlF_6$. The assignment is supported by the inspection of the spectra recorded for the position of ^{19}F resonance line in $(NH_4)_3AlF_6$ (−143 ppm). Moreover, the appearance of XRD peak at $2\theta = 17.3^\circ$ is also characteristic of $(NH_4)_3AlF_6$ phase (see Fig. 1c). On the other hand, the broad resonance due to EFAl species at 13 ppm in the ^{27}Al NMR spectrum corresponds to the broad ^{19}F resonances in the range of −150 to −156 ppm. The small peak at −161 ppm may be due to surface adsorbed SiF_4, or possibly HF_2^- [28]. By washing the dealuminated samples with hot water, all the ^{19}F NMR signal intensities decreased dramatically, which supported the assignments of the above ^{19}F-containing species were not in the framework.

3.7. ^{19}F MAS NMR of H-MOR/AHFS-x-None

The ^{19}F MAS NMR spectra of H-MOR/AHFS-*x*-None are displayed in Fig. 6. For H-MOR/AHFS-2.5-None sample, the peaks at −125 and −130 ppm dominated the spectrum, and multiple lines at −143, −148, −150, −156, and −161 ppm were observed, indicating that a variety of fluoride species were formed. After further increasing AHFS content to $x = 5.0$, the peak at −125 ppm almost disap-

peared, and the intensities of the peaks in the range of −140 to −161 ppm increased (Fig. 6b).

Our study showed that a major peak at −158 ppm was observed for AHFS treated pure silica MCM-41 in the absence of NH_4OAc. Since there is no aluminum present in purely siliceous MCM-41, the peak at −158 ppm must be related to Si–F groups, resulting from the replacement of hydroxyl group in the silanols by fluorine atom, or a terminal fluorine atom at the surface. This implies that fluorination with AHFS resulting in the formation of $(SiO_3)Si–F$ groups, where –F has replaced –OH, cannot be entirely excluded. Moreover, the treatment of Al-MCM-41 with ammonium fluoride leading to the formation of Si–F species at ^{19}F NMR signal at −156 ppm has been reported [29]. Therefore, the peaks in the range of −156 to −158 ppm observed in AHFS treated H-MOR sample, both in the presence and absence of NH_4OAc, can be assigned to Si–F groups. Unfortunately, this signal might be overlapped with those of aluminum fluoro-complexes, and resulted in a broad signal centered at –156 ppm at higher AHFS content (see Figs. 5b and 6b). Thus the quantitative distinction between the fluorine atom in Si–F groups and the aluminum fluoro-complexes appears to be very difficult.

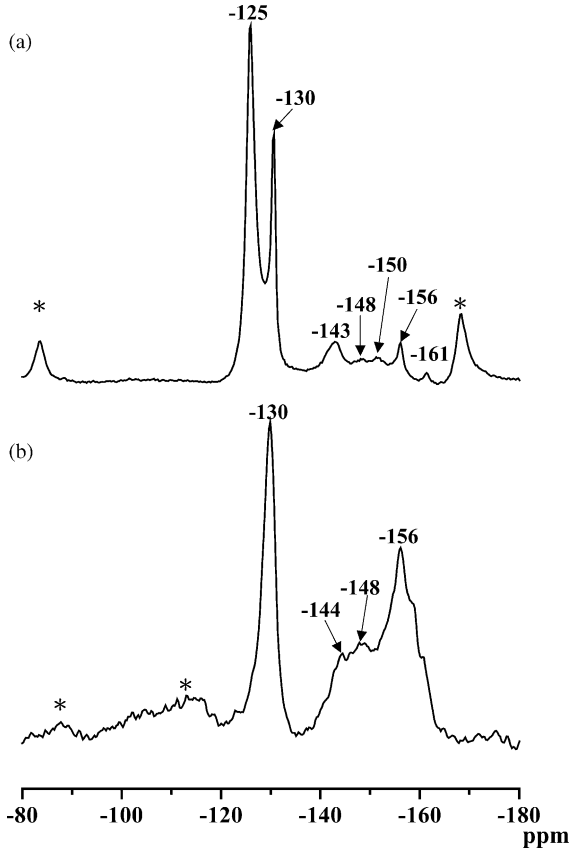

Fig. 6. ^{19}F MAS NMR spectra of H-MOR/AHFS-*x*-None, where *x* is equal to (a) 2.5 and (b) 5.0. Spectra were acquired at a spinning speed of 12 kHz. Asterisks denote spinning sidebands.

3.8. ^{29}Si MAS NMR

The ^{29}Si MAS NMR spectra of dealuminated samples (Fig. 7) show two major resonances centered at around −112 and −105 ppm. The resonance at −112 ppm is assigned to Si(0Al) (Q^4) site. The downfield peak at around –105 ppm is associated with Si atoms in Si(1Al) and Si–OH (Q^3) environments [30]. The contribution from Si atoms associated with hydroxyl groups can be confirmed by the increase in the intensity of the resonance at −105 ppm when ^1H to ^{29}Si cross-polarization (CP) was applied [31]. Although dealumination of the framework took place, as evidenced by ^{27}Al and ^{19}F NMR measurements, the ^{29}Si MAS NMR spectra hardly changed after each AHFS dealumination. Overall, AHFS treatment in the presence of NH_4OAc led to the formation of a larger number of Q^3 sites compared to the case of the absence of NH_4OAc. This is due to the preferential formation of hydroxyl nests (lattice defects) during the former treatment.

3.9. Cumene cracking activity

The acidic properties of H-MOR and its dealuminated samples were further investigated by cumene cracking reactions, and the results were shown in Fig. 8. The conversion of cumene requires medium to strong acid sites of the ma-

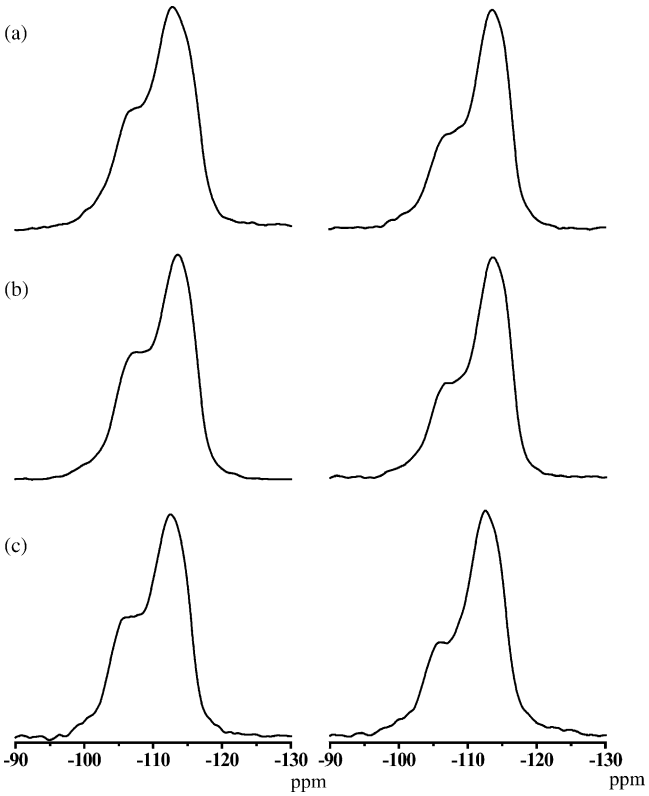

Fig. 7. ^{29}Si MAS NMR spectra of H-MOR/AHFS-*x*-NH_4OAc (left) and H-MOR/AHFS-*x*-None (right), where *x* is equal to (a) 0.5, (b) 1.5, and (c) 2.5.

terials. To evaluate the role of EFAl species governing the acidity, all dealuminated samples were not washed with hot water in order to preserve all EFAl species. All cracking products were only benzene and propene, indicating that the active sites were of Brønsted acid type for all dealuminated samples. As seen in Fig. 8, dealuminated samples showed less (about 10–30% less) cumene cracking activity than the parent H-MOR sample. The AHFS treatment removed Al from the framework position. Hence it decreased the number of Brønsted acid sites. The observed reduction in catalytic activity as a function of time on stream resulted from the increased diffusional resistances caused by the pore blocking due to agglomerates of EFAl species. Overall, the acid strength was higher on H-MOR/AHFS-*x*-NH_4OAc samples than on H-MOR/AHFS-*x*-None samples. This could be ascribed to the elimination of more Al atoms from the framework in H-MOR/AHFS-*x*-NH_4OAc samples, and thus the acidity was enhanced due to a higher Si/Al ratio in the framework. The same trend was observed with increasing AHFS loading for a given type of treatment. The EFAl species seemed to be in a form that did not contribute to the Brønsted acidity. Hence they did not directly affect the activity.

3.10. Nature of the fluorinated species

In the case of H-MOR/AHFS-*x*-NH_4OAc, a comparison of Figs. 2 and 5 indicated that the major ^{19}F resonance at –143 ppm corresponded to the dominant EFAl species resonating at 0 ppm in the ^{27}Al spectrum, and was assigned to $(NH_4)_3AlF_6$. The assignment is consistent with the ^{27}Al and ^{19}F chemical shifts for crystalline $(NH_4)_3AlF_6$, also confirmed by the appearance of XRD peak at $2\theta = 17.3^\circ$ (see Fig. 1c). Besides the peak at –143 ppm, the broad signals in the range of –150 to 156 ppm in the ^{19}F NMR spectra corresponded to the broad ^{27}Al resonance at 13 ppm.

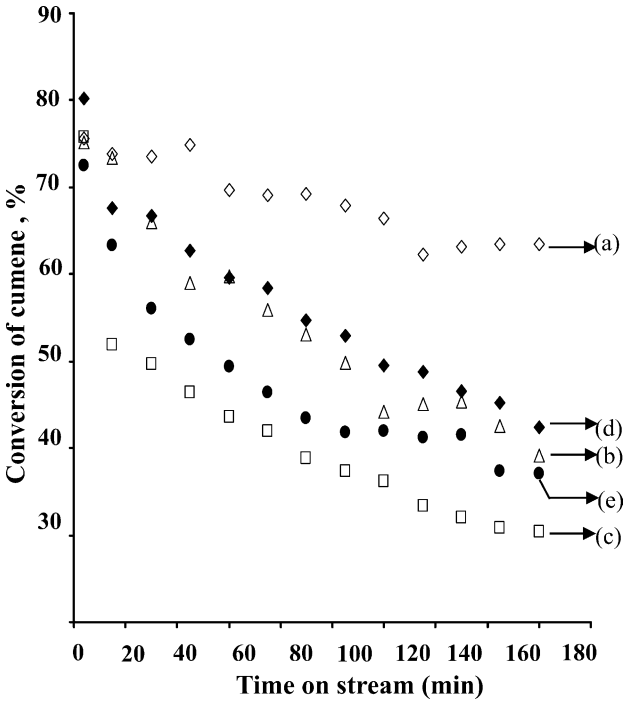

Fig. 8. Cumene conversion curves for (a) H-MOR, (b) H-MOR/AHFS-1.5-NH_4OAc, (c) H-MOR/AHFS-1.5-None, (d) H-MOR/AHFS-5.0-NH_4OAc, and (e) H-MOR/AHFS-5.0-None.

In the case of H-MOR/AHFS-*x*-None sample, the ^{27}Al resonances at 13 ppm, and the pattern spread in the range of −20 to −90 ppm were associated with the ^{19}F resonances at −148, −150, and −156 ppm, respectively (cf. Figs. 3b and 6a). Interestingly, the ^{27}Al NMR signal at 13 ppm was not observed at higher AHFS content ($x = 5.0$, Fig. 3c). As evidenced in the ^{27}Al and ^{19}F NMR spectra of H-MOR/AHFS-5.0-None sample (Figs. 3c and 6b), the ^{27}Al pattern spread in the range of −20 to −90 ppm has to be associated with the multiple ^{19}F peaks in the range of −144 to −148 ppm. The ^{19}F peak observed at −150 ppm for H-MOR/AHFS-2.5-None was no longer resolved for H-MOR/AHFS-5.0-None. The main difference in the ^{27}Al spectra for these two samples was that the ^{27}Al peak at 13 ppm was observed for the former sample but not for the latter sample. Therefore, the multiple lines centered at around −150 ppm were most likely associated with the ^{27}Al peak at 13 ppm. Based on its larger ^{27}Al linewidth as compared to that of the resonance at 0 ppm, it implied that the corresponding aluminum fluoro-complexes exhibited a distribution of different aluminum fluorides. A comparison of Figs. 5a and 6a indicated that the ^{27}Al peak at 13 ppm corresponded to the ^{19}F NMR signals in the range of −150 to −156 ppm.

The observed ^{19}F resonances can be compared with those obtained for complexes in solution. Sur and Bryant [32] have studied fluoroaluminum complexes in solution and adsorbed by zeolites. They have assigned sharp lines from −145 to −156 ppm to complexes such as $[AlF_x(H_2O)_{6-x}]^{(3-x)+}$. In fluorinated alumina, Fischer et al. [33] have observed broad but resolved lines at −154 and −143 ppm that they assigned to $(Al^{VI}O_5F)$ and $(Al^{VI}O_4F_2)$ environments. In the present study, two types of aluminum fluoro-complexes are considered, i.e., $AlF_x(OH)_{3-x(aq)}$ and $[AlF_x(H_2O)_{6-x}]^{(3-x)+}$ ($x = 1$–3). Due to the relative low level of dealumination in H-MOR, it is reasonable that one or two F atoms in aluminum complexes are located at the terminal positions, bonding to only one Al atom. This will also be the guideline for choosing possible EFAl structures in the latter ab initio calculations. Considering the relatively close chemical shift observed for a pseudo-octahedral Al^{3+} in hydrated forms of AlF_3 (at 20 ppm) [32], we assigned the ^{27}Al resonance at 13 ppm to $[AlF_x(H_2O)_{6-x}]^{(3-x)+}$ species, which resulted from the substitution by fluorine of water molecules in the coordination sphere of octahedral aluminum atoms. Based on the low ^{19}F peak intensity as compared to that of $(NH_4)_3AlF_6$ (Fig. 5b), the *x* value is most likely 1 or 2. On the other hand, the ^{27}Al pattern spread from –20 to –90 ppm having a larger quadrupolar coupling can be attributable to aluminum hydroxyfluorides, i.e., $AlF_x(OH)_{3-x(aq)}$, which

were formed from the substitution by fluorine of water molecules in the coordination sphere of octahedral Al–OH groups. One might expect that $AlF_x(OH)_{3-x(aq)}$ species exhibit more distorted environments as compared to $[AlF_x(H_2O)_{6-x}]^{(3-x)+}$ species, and thus experience a stronger quadrupolar coupling. There were a small amount of Al–OH groups present in H-mordenite, as confirmed by $^1H\{^{27}Al\}$ TRAPDOR NMR in our previous study [31]. This provides an indirect support that the pattern spread from −20 to −90 ppm has to be related with Al–OH groups. Martinez et al. [34] reported that the ^{19}F chemical shifts for $[AlF_x(H_2O)_{6-x}]^{(3-x)+}$ and $AlF_x(OH)_{3-x(aq)}$ in the solution are in a similar range of −152 to −156 ppm; the latter species has a downfield shift. In addition, it was reported that the ^{19}F NMR spectrum of AlF_3 in D_2O solution consisted of two peaks at −154 and −155 ppm, which were assigned to $AlF(H_2O)_5^{2+}$ and $AlF_2(H_2O)_4^+$, respectively [35]. Even if the rigorous assignment of these two types of fluoroaluminate complexes seems difficult, as deduced from their similar ^{19}F chemical shifts, discrimination between these different species is feasible by monitoring the change of ^{19}F peak shift as a function of AHFS content. Thus, the ^{19}F resonances in the range of −150 to −156 ppm and −144 to −148 ppm are assigned to $[AlF_x(H_2O)_{6-x}]^{(3-x)+}$ and $AlF_x(OH)_{3-x(aq)}$, respectively, in the AHFS treated H-MOR samples.

3.11. ^{19}F chemical shifts from ab initio calculations

The true nature of EFAl is usually not known even though studies employing different physical methods have been made. As discussed above, two types of EFAL species, namely $[AlF_x(H_2O)_{6-x}]^{(3-x)+}$ and $AlF_x(OH)_{3-x(aq)}$, are the most probable structures in the present case. To help with the above assignment for ^{19}F peaks, therefore, we focused on the ^{19}F NMR shifts calculated from ab intio methods based on these compositions. Since it has been recognized that EFAl species are usually octahedrally coordinated, here we only consider six-coordinated Al species containing terminal F atoms. The extraframework Al species created by dealumination, which are carried out under a water-rich atmosphere, normally have a large affinity for adsorbing water molecules near their location. Therefore, subsequent interaction of the EFAl species with additional water molecules should be highly probable. Thus, we carried out calculations of these two types of extraframework Al species coordinated with water molecules. The optimized structures of some selected Al–F complexes and their corresponding ^{19}F NMR shifts are displayed in Fig. 9. The chemical shielding tensors and isotropic shifts are summarized in Table 1. Considering these two types of EFAl species carrying the same charge, a clear trend in the chemical composition, relative to the F-atom shielding, was found for the *trans* conformation but not for the *cis* conformation. That is, the ^{19}F NMR shift of *trans*-$AlF(OH)(H_2O)_4^+$ tends to be more down-field as compared with that of *trans*-$AlF_2(H_2O)_4^+$, giving the same number of charge of the complexes. This tendency is consistent with the above ^{19}F peak assignment. Since the Al atom in the zeolitic framework induces a negative charge in the framework, these monoionic positive charged EFAl species are highly possible. These ab initio calculation results serve as a guideline toward understanding the exact nature of EFAl species. Although the calculated ^{19}F shift for $AlF(H_2O)_5^{2+}$ species was similar to that of $AlF(OH)(H_2O)_4^+$ species, the former species seemed unlikely to be present inside the zeolite structure due to its higher positive charges. We also found that a complicated situation might occur in different Al coordination (e.g., 4-, 5-, or 6-coordinated) because they will give very different ^{19}F NMR shifts. It was reported that many factors beyond the closest coordination shell of the F atom could significantly affect the ^{19}F NMR properties [19]. The exact nature of EFAl species is more complicated than the proposed chemical compositions. A more detailed study on the effect of the coordination number of aluminum with water molecules and the cluster models using "$OSiH_3$" ligands rather than hydrogen atoms to represent some framework of zeolite network is currently in progress.

3.12. Possible mechanisms of dealumination

The proposed mechanisms of the AHFS dealumination in the presence of NH_4OAc basically involved the extraction of aluminum from the framework leaving a vacancy in which silicon was subsequently inserted. It has been

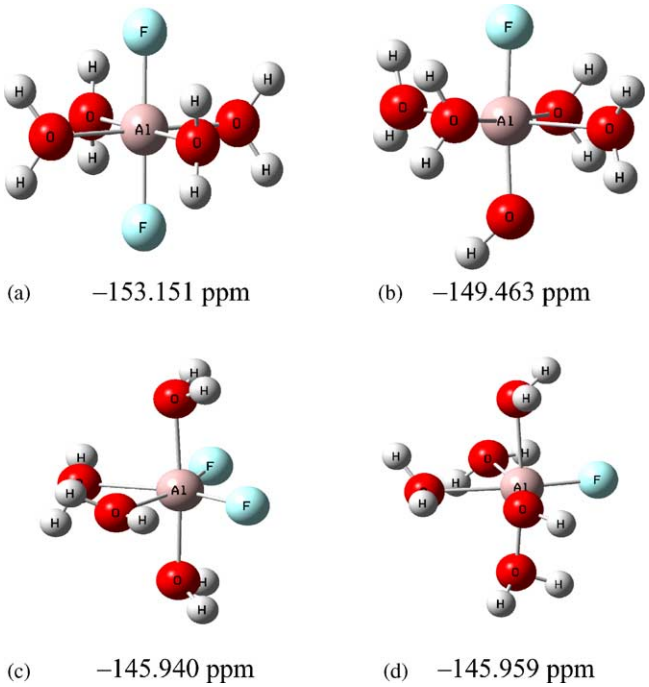

Fig. 9. Ab initio calculations of structures and the corresponding ^{19}F NMR shifts for selected six-coordinated Al species containing terminal F atoms: (a) *trans*-$AlF_2(H_2O)_4^+$, (b) *cis*-$AlF_2(H_2O)_4^+$, (c) *trans*-$AlF(OH)(H_2O)_4^+$, and (d) *cis*-$AlF(OH)(H_2O)_4^+$.

Table 1
^{19}F NMR chemical shielding tensors of selected six-coordinated Al–F complexes

Species	σ_{11}	σ_{22}	σ_{33}	σ_{iso}	δ_{iso}
CCl_3F	212.703	212.746	315.176	246.875	0.0
$AlF(H_2O)_5^{2+}$	377.608	369.859	430.353	392.607	–145.731
$AlF_2(H_2O)_4^{+}$	383.304	383.828	432.945	400.026	–153.151 (*trans*)[a]
	379.497	400.522	398.425	392.815	–145.940 (*cis*)[a]
$AlF(OH)(H_2O)_4^{+}$	380.828	380.197	427.991	396.339	–149.463 (*trans*)
	376.776	391.952	409.776	392.835	–145.959 (*cis*)
$AlF(OH)_2(H_2O)_3$	377.213	380.082	424.004	393.767	–146.891
$AlF_2(OH)(H_2O)_3$	376.029	386.152	431.740	397.974	–151.099[a]
	372.090	385.764	425.920	394.591	–147.716[a]

[a] The two F atoms give very similar isotropic chemical shifts in each conformation.

suggested that aluminum is removed in the form of AlF_6^{3-} ions whereas the inserted species is monomolecular silicic acid $Si(OH)_4$ [7,8]. Our ^{19}F and ^{27}Al NMR results directly confirmed the formation of $(NH_4)_3AlF_6$ species, judging from its signals at 0 ppm in the ^{27}Al spectrum and −143 ppm in the ^{19}F NMR spectrum, respectively. Some variants of $[AlF_x(H_2O)_{6-x}]^{(3-x)+}$ species would be expected to give rise to another type of octahedral Al^{3+} in the ^{27}Al spectrum showing a peak at 13 ppm. Previous studies have shown that different aluminum fluoride species such as $[AlF_x(H_2O)_{6-x}]^{(3-x)+}$ ($x = 1$–5) were formed successively as the concentration of fluoride ion increased. At sufficiently high fluoride ion concentration, an octahedral AlF_6^{3-} species started to form in appreciable amount [35]. At high level of AHFS while the concentration of fluoride ion is sufficiently enough, the preferential formation of $(NH_4)_3AlF_6$ is then expected. Thus, it is concluded that the essential part of the dealumination process carried on with AHFS in the presence of NH_4OAc is that the extracted Al^{3+} reacts with F^- to form $(NH_4)_3AlF_6$ species.

Without adding NH_4OAc, the zeolite solution is acidic (pH ∼3.5). Under such conditions, the zeolite sample is dealuminated by acid leaching induced by AHFS, and thus results in the formation of some amounts of terminal silanols and EFAl species like Al–OH species. In comparison to the case of adding NH_4OAc, however, less silanol groups are formed, as deduced from the results of ^{29}Si NMR and degree of dealumination. In parallel with dealumination, SiF_6^{2-} can be hydrolyzed and then serve as a fluorination reagent, and the resulting fluoride ions react with both terminal silanols and Al–OH moieties of intermediate (transient) products leaving the framework to form Si–F groups and aluminum hydroxyfluorides, respectively. Clearly, the dealumination of H-MOR leading to the formation of $(NH_4)_3AlF_6$ does not become energetically favorable in the absence of NH_4OAc especially for the high AHFS content. It is clear that the control of pH to be near neutral is a key step responsible for the strong preference for the formation of AlF_6^{3-}. In the absence of NH_4OAc, on the contrary, the solution is too acidic to provide enough concentration of fluoride ion to form AlF_6^{3-}, and fluorination of both the silanols at the surface and EFAl species proceed predominantly.

4. Conclusions

The effects of AHFS dealumination in the presence and absence of NH_4OAc on the status and nature of fluorinated EFAl species in H-MOR were investigated. It was found that both treatments were not very effective in removing framework aluminum. The treatment in the presence of NH_4OAc led to more structural defects (silanol groups), as revealed by ^{29}Si NMR. A variety of aluminum fluoro-complexes, most likely $[AlF_x(H_2O)_{6-x}]^{(3-x)+}$ and $AlF_x(OH)_{3-x(aq)}$, were proposed on the basis of observations of ^{27}Al and ^{19}F NMR. Ab initio calculations indicated that the exact nature of EFAl species was more complicated than the proposed chemical compositions.

Acknowledgements

Financial support from the National Science Council of Taiwan is gratefully acknowledged.

References

[1] N.Y. Chen, W.E. Garwood, F.G. Dwyer, Shape Selective Catalysis in Industrial Applications, 2nd ed., Dekker, New York, 1996.
[2] P.A. Parikh, N. Subrahmanyam, Y.S. Bhat, A.B. Halgeri, J. Mol. Catal. 88 (1994) 85.
[3] M. Maache, A. Janin, J.C. Lavalley, J.F. Joly, Zeolites 13 (1993) 419.
[4] M.R. Apellian, A.S. Fung, G.J. Kennedy, T.F. Degnan, J. Phys. Chem. 100 (1996) 16577.
[5] X. Zaiku, Q. Chen, C. Zhang, J. Bao, Y. Cao, J. Phys. Chem. B 104 (2000) 2853.
[6] J. Weitkamp, M. Sakuth, C. Chen, S. Ernst, J. Chem. Soc., Chem. Commun. (1989) 1908.
[7] G.W. Skeels, D.W. Breck, in: D.H. Olson, A. Bisio (Eds.), Proceedings of the Sixth International Zeolite Conference, Butterworths, Surrey, 1983.

[8] D.W. Breck, H. Blass, G.W. Skells, US Patent 45,323 (1985).
[9] C.S. Triantafillidis, A.G. Vlessidis, L. Nalbandian, N.P. Evmiridis, Micro. Meso. Mater. 47 (2001) 369.
[10] W.M. Meier, D.H. Olson, Ch. Baerlocher, Atlas of Zeolite Structure Types, 4th ed., Elsevier, 1996.
[11] J.M. Silva, M.F. Ribeiro, F. Ramoa Ribeiro, E. Benazzi, N.S. Gnep, M. Guisnet, Zeolites 16 (1996) 275.
[12] J. Scherzer, in: T.E. White, R.A. Della Betta, E.G. Derouane, B.T.K. Baker (Eds.), Catalytic Materials: Relationship Between Structure and Activity, ACS Symposium Series 248, Am. Chem. Soc., Washington, DC, 1984, p. 157.
[13] L. Benco, T. Demuth, J. Hafner, F. Hutschka, H. Toulhoat, J. Catal. 209 (2002) 480.
[14] A.A. Sokol, C.R.A. Catlow, J.M. Garcés, A. Kuperman, J. Phys. Chem. B 106 (2002) 6163.
[15] D. Farcasiu, P. Lukinskas, J. Phys. Chem. A 106 (2002) 1619.
[16] G.M. Zhidomirov, A.L. Yakovlev, M.A. Milov, N.A. Kachurovskaya, I.V. Yudanov, Catal. Today 51 (1999) 397.
[17] J.M. Ruiz, M.H. McAdon, J.M. Garcés, J. Phys. Chem. B 101 (1997) 1733.
[18] D.L. Bhering, A. Ramirez-Solis, C.J.A. Mota, J. Phys. Chem. B 107 (2003) 4342.
[19] Y. Liu, J. Tossell, J. Phys. Chem. B 107 (2003) 11280.
[20] D. Fenzke, D. Freude, T. Frohlich, J. Haase, Chem. Phys. Lett. 111 (1984) 171.
[21] M.J. Frisch, G.W. Trucks, H.B. Schlegel, G.E. Scuseria, M.A. Robb, J.R. Cheeseman, V.G. Zakrzewski, J.A. Montgomery Jr., R.E. Stratmann, J.C. Burant, S. Dapprich, J.M. Millam, A.D. Daniels, K.N. Kudin, M.C. Strain, O. Farkas, J. Tomasi, V. Barone, M. Cossi, R. Cammi, B. Mennucci, C. Pomelli, C. Adamo, S. Clifford, J. Ochterski, G.A. Petersson, P.Y. Ayala, Q. Cui, K. Morokuma, D.K. Malick, A.D. Rabuck, K. Raghavachari, J.B. Foresman, J. Cioslowski, J.V. Ortiz, B.B. Stefanov, G. Liu, A. Liashenko, P. Piskorz, I. Komaromi, R. Gomperts, R.L. Martin, D.J. Fox, T. Keith, M.A. Al-Laham, C.Y. Peng, A. Nanayakkara, C. Gonzalez, M. Challacombe, P.M.W. Gill, B.G. Johnson, W. Chen, M.W. Wong, J.L. Andres, M. Head-Gordon, E.S. Replogle, J.A. Pople, Gaussian'98, revision A.9, Gaussian, Inc., Pittsburgh, PA, 1998.
[22] A.D. Becke, J. Chem. Phys. 98 (1993) 5648.
[23] R. Ditchfield, Mol. Phys. 27 (1974) 789.
[24] K. Wolinski, J.F. Hinton, P. Pulay, J. Am. Chem. Soc. 112 (1990) 8251.
[25] L. Frydman, J.S. Harwood, J. Am. Chem. Soc. 117 (1995) 12779.
[26] G. Garralon, V. Fornes, A. Corma, Zeolites 8 (1988) 268.
[27] L. Delmotte, M. Soulard, F. Guth, A. Seive, A. Lopez, J.L. Guth, Zeolites 10 (1990) 778.
[28] T.M. Duncan, J.R. van Wazer, Compilation of Reported ^{19}F NMR Chemical Shifts, Wiley-Interscience, 1970.
[29] M. Xu, W. Wang, M. Seiler, A. Buchholz, M. Hunger, J. Phys. Chem. B 106 (2002) 3202.
[30] G. Engelhardt, D. Michel, High-resolution Solid-state NMR of Silicates and Zeolites, Wiley, New York, 1987.
[31] H.M. Kao, C.Y. Yu, M.C. Yeh, Micro. Meso. Mater. 53 (2002) 1.
[32] S.K. Sur, R.G. Bryant, Zeolites 16 (1996) 118.
[33] L. Fischer, V. Harle, S. Kasztelan, J.B. d'Espinose de la Caillerie, Solid State Nucl. Magn. Reson. 16 (2000) 85.
[34] E.J. Martinez, J.L. Girardet, C. Morat, Inorg. Chem. 35 (1996) 706.
[35] N.A. Matwiyoff, W.E. Wageman, Inorg. Chem. 9 (1970) 1031.